Journal of Applied Physics

High-temperature recrystallization effects in swift heavy ion irradiated $KY(WO_4)_2$

Cite as: J. Appl. Phys. **130**, 185109 (2021); https://doi.org/10.1063/5.0060765
Submitted: 22 June 2021 • Accepted: 18 October 2021 • Published Online: 12 November 2021

R. N. Frentrop, V. Tormo-Marquez, F. B. Segerink, et al.

AIP Publishing

Journal of Applied Physics ARTICLE scitation.org/journal/jap

High-temperature recrystallization effects in swift heavy ion irradiated $KY(WO_4)_2$

Cite as: J. Appl. Phys. **130**, 185109 (2021); doi: 10.1063/5.0060765
Submitted: 22 June 2021 · Accepted: 18 October 2021 ·
Published Online: 12 November 2021

View Online Export Citation CrossMark

R. N. Frentrop,[1,a)] V. Tormo-Marquez,[2] F. B. Segerink,[1] M. C. Pujol,[3] J. Olivares,[2,4] and S. M. Garcia-Blanco[1,b)]

AFFILIATIONS

[1]MESA+ Institute for Nanotechnology, University of Twente, P.O. Box 217, 7500 AE Enschede, The Netherlands
[2]Centro de Micro-análisis de Materiales (CMAM), Universidad Autónoma de Madrid (UAM), 28049 Madrid, Spain
[3]Physics and Cristallography of Materials (FiCMA), Universitat Rovira i Virgili, 43007 Tarragona, Spain
[4]Instituto de Óptica, Consejo Superior de Investigaciones Científicas, (IO, CSIC), C/Serrano 121, 28006 Madrid, Spain

[a)]**Author to whom correspondence should be addressed:** r.n.frentrop@utwente.nl
[b)]**Electronic mail:** s.m.garciablanco@utwente.nl

ABSTRACT

$KY(WO_4)_2$ crystal has a lot of potential as an on-chip waveguide material for lanthanide ion-doped, Raman active lasers and on-chip amplifiers. One method of fabricating these waveguides is by using swift carbon ion irradiation, which produces a step-like, damage-induced refractive index contrast of up to $\Delta n \approx 0.2$. The irradiation is followed by an annealing step to reduce color centers that cause high optical absorption, leading to an optical slab waveguide with optical transmission losses as low as 1.5 dB/cm at 1550 nm. In this article, we report an upper limit of ~450 °C to the annealing temperature, above which stresses and recrystallization induce additional scattering detrimental to waveguide performance. The effects are characterized using transmission electron microscopy and Raman microscopy.

I. INTRODUCTION

The monoclinic potassium double tungstate family [$KY(WO_4)_2$, $KYb(WO_4)_2$, $KLu(WO_4)_2$, $KGd(WO_4)_2$, in short KREW] has been used as a material for bulk Raman and lanthanide ion-doped lasers for decades[1–3] because of its high refractive index, reasonably large thermal conductivity, long inter-ionic distances, and large transition cross sections for rare-earth ions.[4] Recently, many research efforts have been devoted to the fabrication of active, lanthanide ion-doped KREW optical waveguides for the realization of on-chip amplifiers[5] and lasers.[6,7] In its stable, low-temperature (<1025 °C) phase, $KY(WO_4)_2$ has a monoclinic structure belonging to the *C2/c* space group, with lattice constants of $a = 10.6251$ Å, $b = 10.3395$ Å, $c = 7.5494$ Å, and $\beta = 130.7410$ °C.[8] The tungstate complexes in the crystalline structure form chains in the *a*–*c* (010) crystalline plane, linked to each other by single and double oxygen bonds. These single and double bonds give rise to the main Stokes frequencies in the Raman spectrum of the crystal. The Stokes frequencies are very similar among many of the potassium double tungstates.[9] High refractive index contrast waveguides with very small mode effective area are desirable to reduce the pump intensity required to achieve stimulated Raman scattering. However, such highly confined waveguides are difficult to fabricate in crystalline KREW materials.

We have recently reported a method to fabricate high refractive index contrast slab waveguides in $KY(WO_4)_2$ by swift heavy carbon ion irradiation to produce a buried damage-induced refractive index reduction in the crystalline material,[11] which can be tuned in both refractive index contrast and distance from the surface by properly selecting the ion fluence and energy. Thermal annealing repairs the damage induced by irradiation in the waveguide core region (i.e., between the surface until the damage barrier) to reduce propagation losses and restore Raman activity of the created waveguide.

In this work, we study the effect of thermal annealing after irradiation up to a temperature of 550 °C. Above 350 °C, no further significant improvement in optical quality and Raman activity of the guiding layer could be found. A transition in the thermal annealing process at ~ 450 °C has been observed, above which both partial recrystallization with a different crystal structure and stress-induced cracking occur in the damage region. These effects

have been investigated using a combination of confocal Raman microscopy and transmission electron microscopy (TEM). This transition sets a clear limit to the maximum annealing temperature to which the substrates can be subjected, as the cracked, polycrystalline layer naturally induces large amounts of light scattering, which makes the fabricated layer no longer usable as an optical waveguide.

II. EXPERIMENTAL METHODS

The $KY(WO_4)_2$ samples used for this research were acquired from Altechna (LT). All samples have dimensions $10 \times 10 \times 1\,mm^3$, oriented such that the large area (top) surface is aligned with the *a*–*c* plane and the *b*-axis points upward (i.e., orthogonal to the *a*–*c* plane). The surface quality provided by Altechna has an RMS roughness of 1 nm. A scratch was made in the top surface of the samples, parallel to the *c* axis, to prevent cracking of the sample due to irradiation-induced stress. Swift heavy carbon ion irradiation was performed at the Centro de Micro-Análisis de Materiales (CMAM) at the Universidad Autónoma de Madrid (ES) in a 5 MV electrostatic tandem accelerator.[12] During irradiation, the samples were oriented at an angle of 5° to avoid channeling.[13] As the ion beam has a Gaussian shape, the ion beam area was set at least 3× larger than the sample surface to provide an even distribution of the ions over the sample. An ion energy of 12 MeV was chosen so that the maximum of the damage barrier induced by electronic interactions was sufficiently deep and was sufficiently wide to permit characterizing the irradiation effects in detail using (diffraction-limited) confocal Raman microscopy. The ion fluence was set at 3×10^{14} ions/cm^2 so that the maximum electronic stopping force was slightly above the amorphization threshold of 1.8×10^{-3} dpa[11] for $KY(WO_4)_2$ (i.e., gray marked region in Fig. 1). After thermal annealing, the *a*–*b* end-facet of the crystals was polished to allow the characterization of the crystal perpendicular to the irradiation direction using confocal Raman microscopy. Study of the irradiation damage by scanning the end-facet of the sample avoids convolution of the Raman signals of the damaged and undamaged regions. Such overlap would occur if the irradiation-induced damage was studied from the surface of the sample. Additionally, the polished end-facet allowed for the measurement of the refractive index profile of the irradiated region using a micro-reflectivity approach.[14] Polishing was done using a Logitech MP5 (UK) polishing machine with a 40 nm SiO_2 particle slurry. Rounding of the edges of the crystal was avoided by clamping the irradiated crystal between 1 mm thick glass substrates. Additionally, TEM samples were fabricated using focused ion beam (FIB)[15] milling for both direct imaging and electron diffraction measurements.

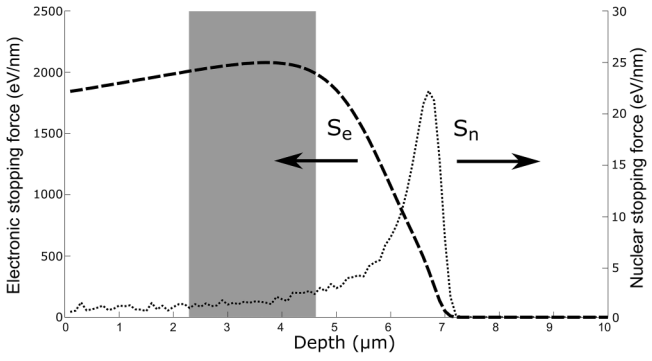

FIG. 1. Electronic and nuclear stopping force curves of 12 MeV carbon ions in $KY(WO_4)_2$ when injected at a 5° angle along the *b*-axis, as simulated by the SRIM-2013 software.[10] The depth is specified as depth into the crystal along the *b*-axis. For a fluence of 3×10^{14} ions/cm^2, the gray area indicates the region above amorphization threshold. The arrows indicate the corresponding axis.

III. RESULTS

A. After irradiation

Initial irradiation with 3×10^{14} ions/cm^2 12 MeV carbon ions/cm^2 produces two regions of damage, namely, a heavy damaged region due to the interaction between the carbon ions and the electron cloud of the crystal (electronic damage), and a damaged region further into the crystal due to the ballistic interaction between the ions and the atoms in the crystal (nuclear damage).[16] In the particular case of this work, the electronic interaction, given by the stopping force, is two orders of magnitude higher than the nuclear damage (see Fig. 1), and no significant contribution of the nuclear damage has been found in previous research.[11,17] The electronic damage in the crystal follows the gradient indicated in Fig. 1, with increasing damage toward the maximum of the electronic stopping force, after which the damage quickly declines. The effect of irradiation on the $KY(WO_4)_2$ structure was studied by TEM, and it is shown in Fig. 2(a) at three different locations in depth, namely, 0.5, 2.5, and 4.5 μm, along the electronic damage curve. In all three locations, a large amorphous fraction, represented by the circular halo, can be observed. Both close to the surface and 2.5 μm below the surface, a deformation of the crystalline structure occurs and it is indicated by the elongated diffraction spots. In the region of highest damage (around 4.5 μm below the surface), the amorphization threshold is reached, resulting in the complete disappearance of any crystalline structure.

Corresponding confocal Raman spectra [Fig. 2(b)] were obtained at the same depth as the TEM images and diffraction patterns and show the same effect. Significant damage can be inferred from the low counts and increasing full-width at half maximum (FWHM) of several of the main Raman peaks associated with $KY(WO_4)_2$ [e.g., the peak at the vibrational 908 cm^{-1} frequency has approximately 4000 counts in unirradiated $KY(WO_4)_2$]. A large amorphous background can be also observed as a broad peak around the frequencies of 360 and 940 cm^{-1}. The signal-to-background ratio (the 908 cm^{-1} peak with the background signal at 850 cm^{-1}) is a good indication of the amount of irradiation damage and emphasizes the severity of the damage, with a ratio of 120 at a depth of 0.5 μm. This signal-to-background lowers to 23 at a depth of 2.5 μm and reduces to values below 1 at 4.5 μm.

Although the damage in the surface region (i.e., 0−3 μm) is severe, a large fraction of this damage consists of point defects or slight torsion of the crystal lattice. These effects are indicated by an increased definition of the amorphous rings in the TEM diffraction patterns, and the elongation of the diffraction spots into lines,

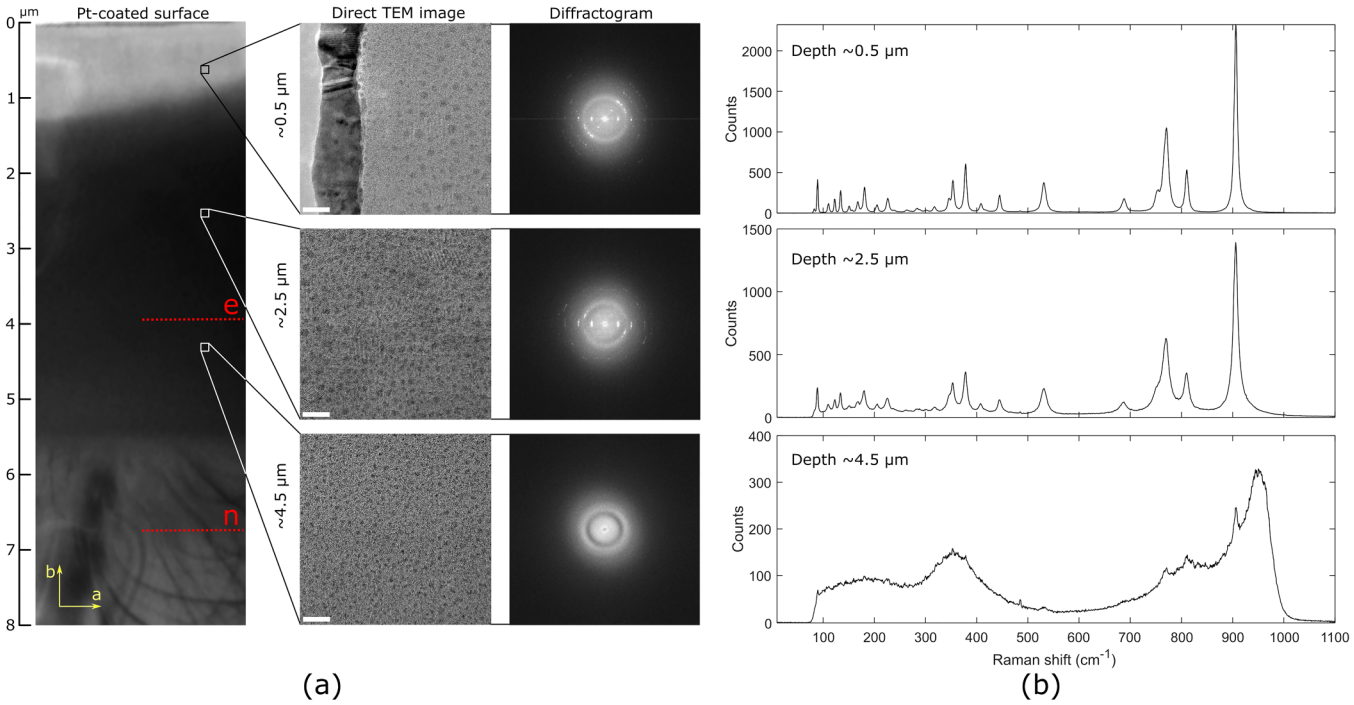

FIG. 2. Analysis of unannealed 12 MeV 3×10^{14} ions/cm^2 carbon-irradiated $KY(WO_4)_2$, showing (a) the TEM cross section and detailed TEM images and diffraction patterns at several depths along the ion path (i.e., 0.5, 2.5, and 4.5 μm) and (b) confocal Raman spectra taken from the end-facets of the irradiated sample at the same distance from the surface as the TEM images. Note the difference in Raman counts for the different regions. The red dashed lines in (a) correspond to the simulated maximum electronic ('e') and nuclear ('n') stopping force. The scale bars in the TEM correspond to 10 nm. The counts of the Raman spectra are calibrated to each other using the background signal at the edges of the frequency range.

respectively. Annealing to 350 °C has shown to be able to repair most of this damage,[11] while the amorphous layer between 3 and 5 μm is consolidated and does not show any sign of repair. Comparing the location of maximum electronic stopping force with the damage region observed in TEM, it should be noted that in TEM, the electronic damage region seems to extend further into the material and the maximum amount of stress is not at the location of maximum stopping force (although the nuclear stopping force and resulting damage are at the same location). The deeper extension of the damage is most likely the result of changing material density during irradiation: the material density of damaged $KY(WO_4)_2$ decreases, causing the location of maximum stopping force to shift further into the material during irradiation.

The refractive index of the irradiated crystal was measured[18] and shows a significant refractive index contrast: at the crystal surface, the refractive index is approximately equal to the unirradiated refractive index ($n = 2.05$ at 1550 nm), while at the maximum of the electronic stopping force it is significantly reduced ($n = 1.86$ at 1550 nm).

B. High-temperature annealing

Annealing above 450 °C shows similar annealing effects in the 0–3 μm surface region, where the amorphization threshold was never reached; TEM images indicate the recovery of the original crystalline structure (see Fig. 3), visible by a reduction of the circular halo and appearance of the characteristic dots related to the unirradiated $KY(WO_4)_2$ lattice. The Raman spectra show recovery toward the spectrum of unirradiated $KY(WO_4)_2$.[11] This can be clearly seen in Fig. 4(a) by a reduction in the FWHM of the 908 cm^{-1} vibrational mode as the annealing temperature increases. Although the FWHM of the 908 cm^{-1} vibrational mode also decreases in the amorphized region (i.e., 3–5 μm) upon annealing, the amplitude of this vibrational mode remains very low throughout the amorphized region after annealing [Fig. 4(b)]. The extension of the electronic damage region that was observed for annealing temperatures below 450 °C is also visible both in TEM and Raman after high-temperature annealing. Additionally, the Raman FWHM indicates that this also means the location of maximum stress is shifted further into the material than the SRIM simulation (indicated by the red dashed line) suggests. It is important to note that even for the high temperatures utilized in this study (i.e., 550 °C), both the FWHM and the electron microscope diffraction patterns indicate that some damage fraction remains in the surface region, which does not recover to the same quality as unirradiated $KY(WO_4)_2$.

In the region above amorphization threshold, where both TEM and Raman microscopy before annealing indicate that the

original $KY(WO_4)_2$ structure was completely lost, a significant change occurs after annealing at temperatures above 450 °C. Instead of further consolidation of the amorphous structure as observed for annealing temperatures up to 450 °C, above this temperature the amorphous structure starts to recrystallize into a polycrystalline region. According to the electron diffraction pattern (Fig. 3), the structure recrystallizes into random orientations but with an overall structure showing a much higher lattice constant. Furthermore, several new vibrational modes that cannot be associated with any of the double tungstate crystals are observed in the Raman spectra obtained at several locations in the recrystallized region (Fig. 4). The steady recovery of the FWHM (but not the amplitude) of the 908 cm^{-1} peak shown in Fig. 4(a) as a function of the annealing temperature indicates partial existence and restoration of the original crystalline structure. Some of the new vibrational modes have been indicated in Fig. 4(b) with their corresponding vibrational frequency. New vibrational modes in the Raman spectrum are observed after annealing at 550 °C, which have also been observed in other single, double, and triple tungstate crystals, when subjected to very high pressures.[19–21] Several of these same vibrational modes can also be found in thermally quenched $KY(WO_4)_2$ [Fig. 4(c)], where part of the material shows a large amorphous Raman background and other parts show vibrational modes at 835, 862, and 970 cm^{-1}, making the composition of thermally quenched $KY(WO_4)_2$ powder very similar to that of the recrystallized barrier. This result seems to suggest that the highly amorphized $KY(WO_4)_2$ material crystallizes in random orientations with a dominant lattice constant that is approximately twice as high as in $KY(WO_4)_2$ (Fig. 2) in a similar way to thermally quenched $KY(WO_4)_2$ powder. Combining the Raman and TEM information, the most likely conclusion is that the original tungstate "sheets" did break up during irradiation and serve as a seed to

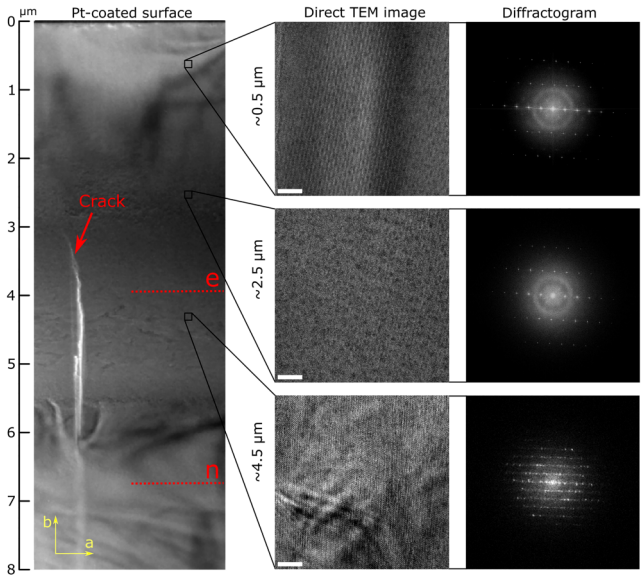

FIG. 3. Analysis of 12 MeV 3×10^{14} ions/cm^2 carbon-irradiated $KY(WO_4)_2$ after annealing the sample at 550 °C. The image shows the TEM cross section and detailed images and diffraction patterns at several locations along the ion path (i.e., 0.5, 2.5, and 4.5 μm). The scale bars in the TEM details indicate a distance of 10 nm.

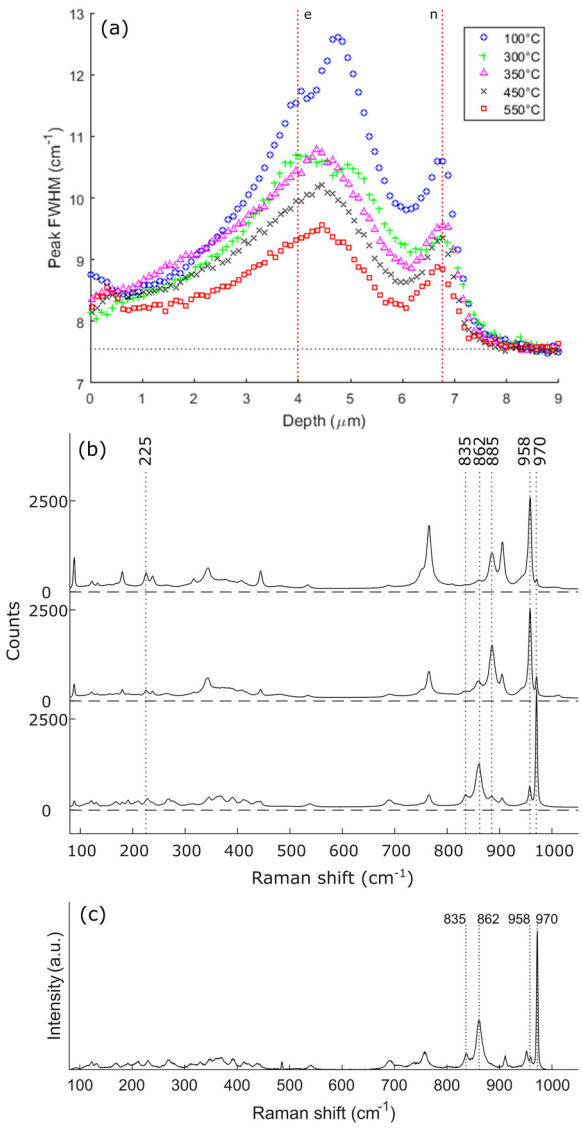

FIG. 4. Analysis of 12 MeV 3×10^{14} ions/cm^2 carbon-irradiated $KY(WO_4)_2$ after thermally annealing the sample at 550 °C. (a) Full width at half maximum of the strongest vibrational mode of $KY(WO_4)_2$ at 908 cm^{-1} as a function of depth in the crystal for different annealing temperatures. The horizontal dashed line indicates the FWHM of the mode in unirradiated $KY(WO_4)_2$. (b) Confocal Raman spectrum at several random locations around the maximum of the electronic damage. (c) Representative confocal Raman spectrum of thermally quenched $KY(WO_4)_2$ powder. In (b) and (c), several frequencies not belonging to low temperature $KY(WO_4)_2$ have been highlighted.

form new tungstate complexes during the high temperature (above 450 °C) annealing step.

These structural changes can also be observed from the refractive index in the electronic damage region, which after annealing at 550 °C was determined using an m-lines scan as $n \approx 1.78$ at 1550 nm. This is significantly lower than for annealing temperatures up to 450 °C. But although this higher refractive index contrast between the surface region and the electronic damage region would be beneficial for the development of on-chip amplifiers and lasers in $KY(WO_4)_2$—as it increases the optical confinement—the clear polycrystalline nature of the electronic damage region also introduces severe scattering. No optical guiding can be observed in the irradiated crystal after annealing at 550 °C for wavelengths up to 1550 nm.

Figure 3 shows the presence of a crack in the region where maximum electronic damage has occurred. Figure 5 shows an overview of the cracks that have formed in the irradiated sample upon annealing at 550 °C. Vertical cracks occur every few micrometers through the entire crystal and generally run parallel to the *a* axis. This effect has been documented before as a result of significant differences in the thermal expansion coefficient between the crystalline axes of $KY(WO_4)_2$[22] or stress between layers of different compositions or crystalline structures due to lattice mismatch.[7] In the high-temperature annealed irradiated crystals, the cracking is most likely the result of a mix of both effects because recrystallization happens at a high temperature and the resulting crystallites exhibit a different structure than the original crystal lattice. Experimentally it is very hard to confirm whether cracking of the recrystallized layer happens during the annealing itself or subsequent cooling step to room temperature. A larger amount of minor cracks and defects, typically aligned in the horizontal direction, are also found in the layer and are the result of a combination of lattice mismatches between the recrystallized regions and edge defects due to the irradiation damage.

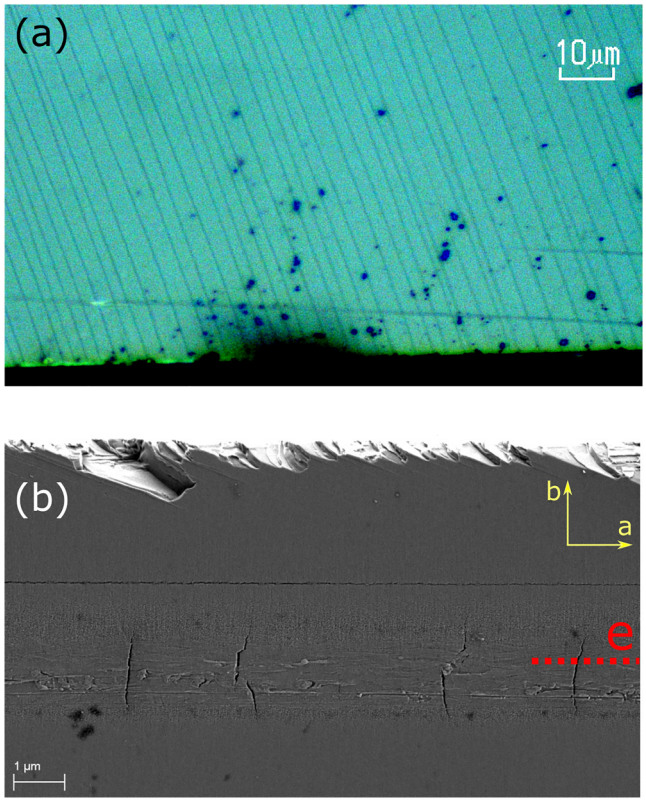

FIG. 5. Cracks appearing in the $KY(WO_4)_2$ after irradiation with 12 MeV 3×10^{14} ions/cm^2 carbon ions and subsequent annealing at 550 °C. (a) Bright-field top-view microscope image showing cracks that run parallel over the entire sample. (b) Scanning electron microscopy (secondary electron) image of the *a*–*b* end-facet showing that the cracks are not present throughout the crystal but only in a region around the maximum of the electronic stopping force (red dashed line). The amorphous layer has recrystallized and cracked, resulting in major cracks perpendicular to the amorphous layer and smaller holes and cracks throughout the layer in random orientations.

IV. CONCLUSION

In summary, although annealing is a necessary step in the waveguide fabrication process for the reduction in color centers in carbon ion-irradiated $KY(WO_4)_2$, there is a limit in terms of annealing temperature that can be used for this process. For waveguides in $KY(WO_4)_2$ fabricated using an irradiation fluence that exceeds the amorphization threshold, annealing above 450 °C has an adverse effect on the quality of the slab waveguide due to recrystallization of the amorphous layer together with stress-induced cracking. The recrystallization does not repair the original crystalline structure but rather creates a layer of crystallites that most likely form from small tungstate complexes that survived the carbon irradiation. This is concluded from the observation of several new vibrations in the Raman spectrum that can be associated with vibrational modes of other tungstate crystals as well as cracking, which is most likely caused by the lattice mismatch induced by the new crystalline phase induced in the amorphized region upon high temperature annealing. The refractive index contrast between the—relatively undamaged—top region and the electronic damage region is increased ($\Delta n = 0.2$ to $\Delta n = 0.25$), but due to the increase in optical scattering and the cracking of the material, the optical losses are much too high to allow optical guiding in the top layer. The immediate conclusion of this study is that for the fabrication of optical waveguides, carbon-irradiated $KY(WO_4)_2$ can only be annealed up to a temperature of 450 °C to avoid recrystallization of the barrier and the corresponding detrimental effects to the performance of the waveguide.

ACKNOWLEDGMENTS

We would like to thank the operators of the MESA+ Institute for Nanotechnology of the University of Twente for their indispensable help in obtaining the transmission electron microscope images and their general support. We also thank the Technical Staff of the CMAM-UAM center for their support with the irradiations. This research was not possible without the funding from the Horizon 2020 European Research Council programme through

Grant No. 648978 and the Comunidad de Madrid through the grant TECHNOFUSION(III)-CM (No. S2018/EMT-4437).

AUTHOR DECLARATIONS

Conflict of Interest

The authors have no conflicts to disclose.

DATA AVAILABILITY

The data that support the findings of this study are available from the corresponding author upon reasonable request.

REFERENCES

[1]A. A. Kaminskii, P. V. Klevtsov, L. Li, and A. A. Pavlyuk, "Stimulated emission from $KY(WO_4)_2$: Nd^{3+} crystal laser," Phys. Status Solidi A **5**, K79–K81 (1971).
[2]V. Petrov, M. C. Pujol, X. Mateos, O. Silvestre, S. Rivier, M. Aguiló, R. M. Solé, J. Liu, U. Griebner, and F. Díaz, "Growth and properties of $KLu(WO_4)_2$, and novel ytterbium and thulium lasers based on this monoclinic crystalline host," Laser Photonics Rev. **1**, 179–212 (2007).
[3]Z. Cong, Z. Liu, Z. Qin, X. Zhang, H. Zhang, J. Li, H. Yu, and W. Wang, "LD-pumped actively Q-switched Nd:$KLu(WO_4)_2$ self-Raman laser at 1185 nm," Opt. Laser Technol. **73**, 50–53 (2015).
[4]M. Pollnau, Y. E. Romanyuk, F. Gardillou, C. N. Borca, U. Griebner, S. Rivier, and V. Petrov, "Double tungstate lasers: From bulk toward on-chip integrated waveguide devices," IEEE J. Select. Top. Q. Electron. **13**, 661–671 (2007).
[5]D. Geskus, S. Aravazhi, S. M. García-Blanco, and M. Pollnau, "Giant optical gain in a rare-earth-ion-doped microstructure," Adv. Mater. **24**, OP19–OP22 (2012).
[6]D. Geskus, E. H. Bernhardi, K. van Dalfsen, S. Aravazhi, and M. Pollnau, "Highly efficient Yb^{3+}-doped channel waveguide laser at 981 nm," Opt. Express **21**, 13773–13778 (2013).
[7]S. Aravazhi, D. Geskus, K. Van Dalfsen, S. A. Vázquez-Córdova, C. Grivas, U. Griebner, S. M. García-Blanco, and M. Pollnau, "Engineering lattice matching, doping level, and optical properties of $KY(WO_4)_2$:Gd, Lu, Yb layers for a cladding-side-pumped channel waveguide laser," Appl. Phys. B: Lasers Opt. **111**, 433–446 (2013).
[8]E. Gallucci, C. Goutaudier, G. Boulon, M. T. Cohen-Adad, and B. F. Mentzen, "Nonstoichiometric $KY(WO_4)_2$: Crystal growth, chemical and physical characterization," J. Cryst. Growth **209**, 895–905 (2000).
[9]A. A. Kaminskii, K. Ueda, H. E. Eichler, J. Findeisen, S. N. Bagayev, F. A. Kuznetsov, A. A. Pavlyuk, G. Boulon, and F. Bourgeois, "Monoclinic tungstates $KDy(WO_4)_2$ and $KLu(WO_4)_2$—New $\chi^{(3)}$-active crystals for laser Raman shifters," Jpn. J. Appl. Phys. Part 2-Lett. **37**, L923–L926 (1998).
[10]J. F. Ziegler, M. D. Ziegler, and J. P. Biersack, "SRIM—The stopping and range of ions in matter (2010)," Nucl. Instrum. Methods Phys. Res. B **268**, 1818–1823 (2010).
[11]R. Frentrop, I. Subbotin, F. Segerink, R. Keim, V. Tormo-Marquez, J. Olivares, K. Shcherbachev, S. Yakunin, I. Makhotkin, and S. M. Garcia-Blanco, "In-depth structural analysis of swift heavy ion irradiation in $KY(WO_4)_2$ for the fabrication of planar optical waveguides," Opt. Mater. Express **9**, 4796 (2019).
[12]A. Redondo-Cubero, M. J. Borge, N. Gordillo, P. C. Gutiérrez, J. Olivares, R. Pérez Casero, and M. D. Ynsa, "Current status and future developments of the ion beam facility at the centre of micro-analysis of materials in Madrid," Eur. Phys. J. Plus **136**, 1–16 (2021).
[13]M. T. Robinson and O. S. Oen, "The channeling of energetic atoms in crystal lattices," Appl. Phys. Lett. **2**, 30–32 (1963).
[14]S. G. Blanco, J. S. Aitchison, C. Hnatovsky, and R. S. Taylor, "Microreflectivity characterization of the two-dimensional refractive index distribution of electron-beam-written optical waveguides in germanium-doped flame-hydrolysis silica," Appl. Phys. Lett. **85**, 1314–1316 (2004).
[15]J. Mayer, L. A. Giannuzzi, T. Kamino, and J. Michael, "TEM sample preparation and FIB-induced damage," MRS Bull. **32**, 400–407 (2007).
[16]O. Peña-Rodróguez, J. Olivares, M. Carrascosa, Á. García-Cabañes, A. Rivera, and F. Agulló-López, "Optical waveguides fabricated by ion implantation/irradiation: A review optical waveguides fabricated by ion implantation/irradiation: A review," in *Ion Implantation*, edited by M. Goorsky (IntechOpen, Rijeka, 2012), Chap. 12.
[17]A. García-Navarro, J. Olivares, G. García, F. Agulló-López, S. García-Blanco, C. Merchant, and J. S. Aitchison, "Fabrication of optical waveguides in KGW by swift heavy ion beam irradiation," Nucl. Instrum. Methods Phys. Res. B **249**, 177–180 (2006).
[18]R. N. Frentrop, V. Tormo-Márquez, J. Olivares, and S. M. García-Blanco, "High-contrast slab waveguide fabrication in $KY(WO_4)_2$ by swift heavy ion irradiation," Proc. SPIE **10535**, 105350O (2018).
[19]W. L. Zhu, K. S. Wan, Y. L. Huang, X. Q. Feng, and G. Pezzotti, "Stress dependence of Raman vibrational bands of $PbWO_4$ single crystals," Phys. Status Solidi A **203**, 2376–2385 (2006).
[20]F. J. Manjon, D. Errandonea, N. Garro, J. Pellicer-Porres, J. Lopez-Solano, P. Rodriguez, S. Radescu, A. Mujica, and A. Munoz, "Lattice dynamics study of scheelite tungstates under high pressure II. $PbWO_4$," Phys. Rev. B **74**, 144112 (2006).
[21]L. J. Burcham and I. E. Wachs, "Vibrational analysis of the two non-equivalent, tetrahedral tungstate (WO_4) units in $Ce_2(WO_4)_3$ and $La_2(WO_4)_3$," Spectrochim. Acta Part A: Mol. Biomol. Spectrosc. **54**, 1355–1368 (1998).
[22]C. I. van Emmerik, R. Frentrop, M. Dijkstra, F. Segerink, R. Kooijman, M. Muneeb, G. Roelkens, E. Ghibaudo, J.-E. Broquin, and S. M. Garcia-Blanco, "Heterogeneous integration of $KY(WO_4)_2$-on-glass: A bonding study," OSA Continuum **2**, 2065 (2019).